Organic & Biomolecular Chemistry

RSC Publishing

PAPER

View Article Online
View Journal | View Issue

Cite this: *Org. Biomol. Chem.*, 2013, **11**, 7789

Evaluating minimalist mimics by exploring key orientations on secondary structures (EKOS)†

Dongyue Xin,[a] Eunhwa Ko,[a] Lisa M. Perez,[b] Thomas R. Ioerger[c] and Kevin Burgess*[a]

Peptide mimics that display amino acid side-chains on semi-rigid scaffolds (not peptide polyamides) can be referred to as minimalist mimics. Accessible conformations of these scaffolds may overlay with secondary structures giving, for example, "minimalist helical mimics". It is difficult for researchers who want to apply minimalist mimics to decide which one to use because there is no widely accepted protocol for calibrating how closely these compounds mimic secondary structures. Moreover, it is also difficult for potential practitioners to evaluate which ideal minimalist helical mimics are preferred for a particular set of side-chains. For instance, what mimic presents *i*, *i* + 4, *i* + 7 side-chains in orientations that best resemble an ideal α-helix, and is a different mimic required for a *i*, *i* + 3, *i* + 7 helical combination? This article describes a protocol for fitting each member of an array of accessible scaffold conformations on secondary structures. The protocol involves: (i) use quenched molecular dynamics (QMD) to generate an ensemble consisting of hundreds of accessible, low energy conformers of the mimics; (ii) representation of each of these as a set of Cα and Cβ coordinates corresponding to three amino acid side-chains displayed by the scaffolds; (iii) similar representation of each combination of three side-chains in each ideal secondary structure as a set of Cα and Cβ coordinates corresponding to three amino acid side-chains displayed by the scaffolds; and, (iv) overlay Cα and Cβ coordinates of all the conformers on all the sets of side-chain "triads" in the ideal secondary structures and express the goodness of fit in terms of root mean squared deviation (RMSD, Å) for each overlay. We refer to this process as *Exploring Key Orientations on Secondary structures* (EKOS). Application of this procedure reveals the relative bias of a scaffold to overlay on different secondary structures, the "side-chain correspondences" (*e.g. i*, *i* + 4, *i* + 7 or *i*, *i* + 3, *i* + 4) of those overlays, and the energy of this state relative to the minimum located. This protocol was tested on some of the most widely cited minimalist α-helical mimics (**1–8** in the text). The data obtained indicates several of these compounds preferentially exist in conformations that resemble other secondary structures as well as α-helices, and many of the α-helical conformations have unexpected side-chain correspondences. These observations imply the featured minimalist mimics have more scope for disrupting PPI interfaces than previously anticipated. Finally, the same simulation method was used to match preferred conformations of minimalist mimics with actual protein/peptide structures at interfaces providing quantitative comparisons of predicted fits of the test mimics at protein–protein interaction sites.

Received 14th June 2013,
Accepted 20th September 2013

DOI: 10.1039/c3ob41848k

www.rsc.org/obc

Introduction

Semi-rigid scaffolds that express amino acid side-chains are interesting chemotypes because these "minimalist mimics"[1] of secondary structure motifs have the potential to disrupt protein–protein interactions (PPIs). They have this potential because PPI interfaces are dominated by side-chain to side-chain contacts[2] hence semi-rigid small molecules that project side-chains in similar orientations to one protein component might competitively interact with the protein-binding partner. Minimalist mimics do not have peptidic polyamide backbones so they are not degraded by proteases and tend to have improved cell- and oral-bioavailabilities relative to peptides.[3]

[a]*Department of Chemistry, Texas A & M University, Box 30012, College Station, TX 77842, USA. E-mail: burgess@tamu.edu*
[b]*Laboratory for Molecular Simulation, Texas A & M University, Box 30012, College Station, TX 77842, USA*
[c]*Department of Computer Science, Texas A & M University, College Station, TX 77843-3112, USA*

†Electronic supplementary information (ESI) available: QMD and matching procedures, overlay data for mimics on ideal secondary structures, scatter plots of RMSD values of conformers *vs.* Δ*E* for mimics, graphics of best fitting mimics on PPIs, sequence correspondence for preferred mimic conformations overlaid on PPI components. See DOI: 10.1039/c3ob41848k

Chronologically, scaffolds **1**,[4–6] **2**,[7] **3**,[8–10] **4**,[11,12] **5**,[13] **6**,[14] **7**,[15] and **8**[16] (Fig. 1) were reported as mimics of helical secondary structures, and are typical of ones in the literature.[17–19] Our interest in the concept of "universal mimics", wherein several secondary structures are represented in one conformational ensemble,[20] led us to wonder if scaffolds that had been described only as α-helical mimics might also be able to access conformers that match other secondary structures. None of the α-helical mimics **1–8** have been claimed to orient side-chains in ways that resemble the less common 3_{10}- and π-helical motifs, but it seemed possible that they could at least do this. Moreover, there is another important issue that it is convenient to refer to here as *side-chain correspondence*; by this we mean the particular side-chains in a secondary structure that best overlay on an accessible conformation of a minimalist mimic. For instance, a scaffold that rigidly presents side-chains in an *i*, *i* + 4, *i* + 7 orientation has that *side-chain correspondence*, whereas it might be unsuitable as a mimic of *i*, *i* + 3, *i* + 4 helical motifs because this is a different *side-chain correspondence*. When evaluating molecules to perturb different protein–protein interfaces it is at least highly desirable, and probably essential, to have a selection of mimics that cover a range of possible side-chain correspondences, and it is important to understand what these are for a given mimic. Of course, the community working in this area is well aware of the need to use the correct side-chain correspondences, but there is no rigorous, systematic approach to assessing what they are for a particular minimalist mimic.

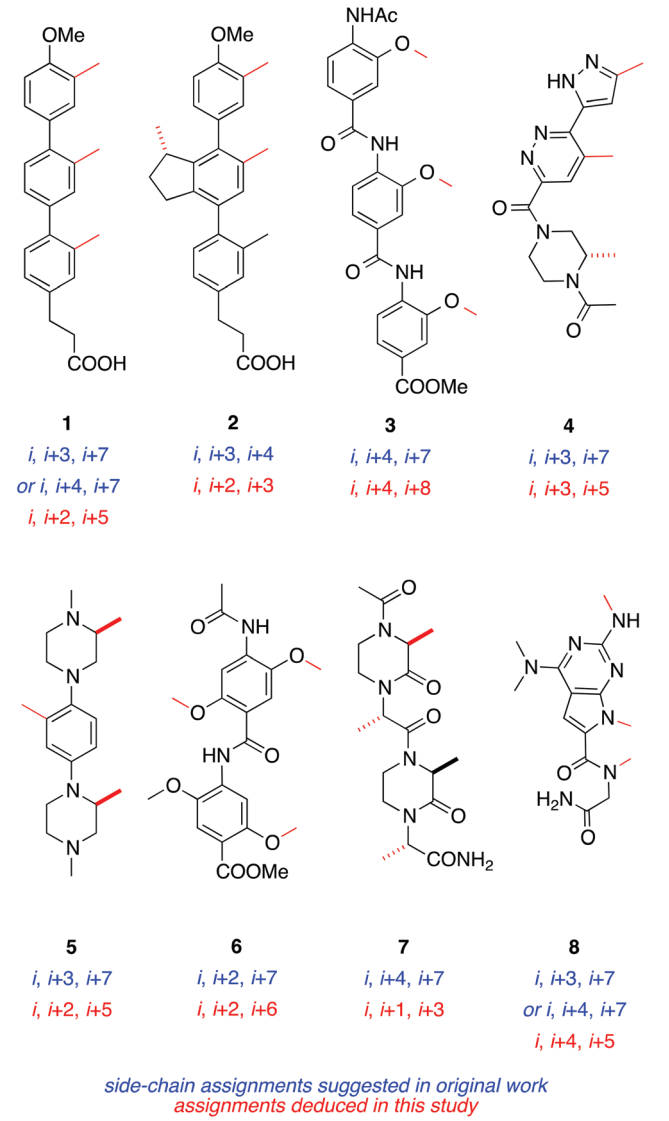

Fig. 1 Helical mimics featured in this paper.

After a side-chain correspondence has been determined, there needs to be a standard parameter to gauge how each minimalist helical mimics fits on that particular side-chain combination. For instance, if two mimics orient *i*, *i* + 3, *i* + 7 side-chains in an ideal α-helical conformation, which one does it most closely? What are the best minimalist mimics to present side-chains in *i*, *i* + 3, *i* + 4 and *i*, *i* + 4, *i* + 7 orientations corresponding to an ideal 3_{10}-helix? Questions like these are difficult to answer using the approaches that have been employed in the literature so far; currently there is no widely accepted method to evaluate the bias of a given scaffold toward a particular conformation. One objective of this paper is to propose a strategy that is applicable to this issue.

Several *experimental* methods have been applied in the context of elaborating equilibrating conformations of minimalist mimics in solution, but none of them, or any combination of them, are suitable for determining the side-chain correspondences and goodness of fit of helical mimics. Broadly speaking these are methods to observe the mimics in solution (*e.g.* NMR and CD), and crystallography.

Arora's study of helical mimic **7**[15] illustrates what direct spectroscopic evidence can be collected to characterize equilibrating conformational states of a minimalist mimic in solution. Circular dichroism (CD) of the molecules **7** in methanol and in acetonitrile had a similar shape to ones for peptide helices, but the minima were red-shifted by 10 nm. NOE experiments were conducted on one compound (actually, in $CDCl_3$), and cross peaks that correspond to the *trans*-isomer, but not the *cis*-one, were observed. However, in solution, minimalist mimics exist as rapidly equilibrating conformational states for which CD and NOE data are *averaged*. In NMR, NOE cross peaks over-represent close contacts relative to distal ones because of the inverse six-power distance relationship; consequently, poorly populated states can appear to be more abundant than prevalent ones. Moreover, some NOE cross peaks for molecules of approximately this molecular mass can be vanishingly small, so absence of cross peaks does not prove that the corresponding conformation is unpopulated; ROESY spectra can help with this, but they have to be carefully calibrated to the properties of the molecule.[21,22] In any case, minimalist mimics *definitely* have multiple conformations, so it is very difficult to unravel which sets of NOE crosspeaks, or CD ellipticities, are associated with individual ones. Consequently, *none of the techniques often used*[10,23,24] *give detailed information on the ensemble of preferred conformations in solution*.

Researchers often turn to crystallography to elucidate conformations of minimalist mimics. Crystallography reveals only a few conformations at best, and these may not be representative of favored ones in solution because of crystal packing forces. Nevertheless, crystallography may provide circumstantial evidence that desired solution states can be accessed, and this type of conclusion is most convincing when molecules crystallize in a conformation that is anticipated to be strongly preferred in solution. This is true of the benzamide mimics **3** and **6** where *H*-bonding between the amide-*NH* and the 2-methoxy substituent is expected to disfavor rotation about the aryl-*NH* bond, and X-ray structures show this.[25,26] Similarly, an X-ray crystal structure of one of Hamilton's terphenyls was obtained to reveal a relevant *solid state* conformation.[6] However, minimalist mimics sometimes crystallize in conformations that are not relevant for secondary structure mimicry. Single crystal X-ray studies reported in a recent contribution from Hamilton, for example, describe how a scaffold that is putatively a sheet mimic in solution crystallizes in some other conformation.[27] In summary, *crystallography does not characterize rapidly equilibrating conformational ensembles of minimalist mimics in solution*.

Given that there seems to be no experimental strategy to characterize equilibrating conformations of minimalist mimics in solution, researchers often turn to calculations. Hamilton's terphenyls **1** were originally conceived to match *i*, *i* + 3, *i* + 7 side-chains on an ideal α-helix (though he has used it as an *i*, *i* + 4, *i* + 7 mimic on some actual helices in PPIs).[4,6] To validate that design his group used Still's Macromodel[28] to simulate some of the preferred trimethyl-substituted terphenyl conformers, and focused on an accessible state that had similar angular projections to the *i*, *i* + 3, *i* + 7 side-chains of an ideal (all-Ala) α-helix. Incidentally, it is relevant to what follows in this work that they observed their simulated structure had 4–25% shorter distances than was optimal, and that the root mean square deviation (RMSD) of the overlay based on Cα–Cβ coordinates was 0.85 Å.[6] Similarly, Arora's hypothesis for α-helical mimicry by **7** is based on modeling of that scaffold using Macromodel (MMFF force field in chloroform). In both the Arora and Hamilton work, the existence of one preferred helical conformer supports the assertion that the scaffold is an α-helical mimic,[29] but this does not comment on the other equilibrating conformations in solution. In other work, researchers have used molecular dynamics simulations on mimics **3** to determine if and how these molecules might bind a groove in the p53 protein that recognizes a helical motif on MDM2,[30] and for the free mimic in water.[31] These studies were not performed with the objective of simulating the ensemble of preferred conformers but instead were used to search for one desired conformer. All these approaches are intended to find particular conformations of putative helical mimics. Such computational strategies sample multiple conformations, but only select certain favored states for analyses.

Near the beginning of this introduction, three important parameters were outlined for evaluating how minimalist mimics can match ideal secondary structures. Essentially these involve considering every accessible member of a representative conformational ensemble for: (i) overlay of conformers on various secondary structures; (ii) side-chain correspondences; and, (iii) goodness of fit. Conveniently, scaffolds **1–8** are relatively rigid, so the calculated bond lengths and angles for each particular conformation are likely to be reliable relative to more complex and flexible structures (*e.g.* peptides); in other words, simulated conformers of these molecules tend to be quite realistic. However, it is very important to recognize the importance of generating and considering a large set of conformers for these molecules; this is because conformers that are quite similar can project side-chains in significantly different ways. For example, sampling a 360° *aryl–aryl* rotation in terphenyls **1** in 1° increments gives a continuum of 360 states, most of which are accessible at room temperature in solution. Within that group of conformers, a difference of only a few degrees in the torsion angle will give significantly different side-chain orientations. Consequently, for the purposes of this work, where most of the accessible side-chain orientations should be considered, it is important to avoid computational approaches that minimize and cluster accessible conformations into families representing local minima. Methods based on Monte Carlo or molecular dynamics with simulated annealing would be inappropriate here. In summary, minimizing routines that cause conformations to converge on local minima are unsuitable for simulating conformational *ensembles* of minimalist mimics.

A representative conformational ensemble for a minimalist mimic might involve hundreds of conformations, all of which are significantly populated, *i.e.* within, for instance, 3 kcal mol^{-1} of the minimum energy conformer located. It is necessary to match each of those conformations on every three amino acid side-chain combination in every common secondary structure to characterize how a minimalist mimics fits, *i.e.* to evaluate the three parameters that reveal how minimalist mimics can match ideal secondary structures; this is a data mining problem rather than a modeling issue. It requires specialized algorithms similar to those we already developed for Exploring Key Orientations (EKO) in protein–protein interactions.[32]

On the basis of the considerations outlined above, we devised a strategy to evaluate how accessible conformations of minimalist mimics match a collection of idealized secondary structures. This strategy consist of the following steps:

(i) use quenched molecular dynamics (QMD) to generate an ensemble consisting of hundreds of accessible, low energy conformers of the mimics;

(ii) represent each of these as a set of Cα and Cβ coordinates corresponding to three amino acid side-chains displayed by the scaffolds;

(iii) represent each combination of three side-chains in each ideal secondary structure as a set of Cα and Cβ coordinates corresponding to three amino acid side-chains displayed by the scaffolds; and,

(iv) overlay Cα and Cβ coordinates of all the conformers on all the sets of side-chain "triads" in the ideal secondary

structures and express their goodness of fit in terms of root mean squared deviation (RMSD, Å) for each overlay.

The strategy outlined above is different to the EKO process[32] which explores key orientations at protein–protein interfaces and is not concerned with secondary structure classifications. However, the strategy outlined here is similarly motivated and facilitated by the process of data mining a conformational ensemble on target structures, so we refer to it as *Exploring Key Orientations on Secondary structures* (EKOS). To the best of our knowledge, it is fundamentally different to any computational approach that has been applied to evaluate minimalist mimics to date. EKOS has the considerable advantage that every accessible conformer in large conformational ensemble is evaluated on every side-chain triad in every secondary structure, and the results are systematically ranked in terms of goodness of fit.

In this work, we focus on the α-helical mimics **1–8** using EKOS to enable quantitative evaluations of solution state structures that are not conveniently possible *via* spectroscopy or other methods. Smith's β-sheet scaffold **9**,[33] and an interface mimic **10** developed on our laboratory[34] were used as "controls" in this study. Scaffold **10** has already been shown to analog several secondary structures with a bias towards β-sheets and, relatively speaking, no notable inclination to mimic helical structures.

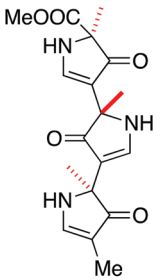

9
sheet mimic
i, *i*+1, *i*+2
i, *i*+1, *i*+2

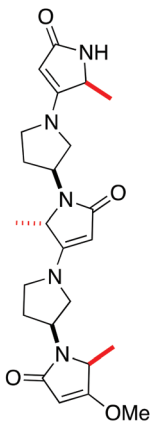

10
sheet mimic
i, *i*+4, *i*+8

Throughout these discussions it is important to remember that helical mimicry is only a means to an end: to use these compounds to displace a protein or peptide that has a helical conformation at a PPI interface. In specific applications of this kind, mimicry of ideal helices is less important than matching the actual helical structure at the interface, which can be distorted and non-ideal. Consequently, even though this study is primarily about evaluating *ideal* helical mimics in general, we have also used EKO to compare the accessible conformations of the helical mimics with helical structures in some of the PPIs that have been perturbed using these mimics. The objective of that part of the study was to ascertain how well scaffolds **1–8** may fit on some well-studied helices in PPIs and compare this with the data for ideal helical mimics.

Results and discussion

Bases for comparison: ideal secondary structures and how to compare them

Secondary structures at protein–protein interfaces are rarely ideal. α-Helices, for instance, can be stretched, compressed, bent, kinked, and partially unwound. In the minimalist mimic area, the most direct approach to designing a scaffold to specifically perturb a particular PPI is to match the secondary structures at that interface, including their distortions and other peculiarities. However, it is often logical to begin the process of mimicking a real helical motif with the most closely related *ideal* helical mimic. Recognizing this, a significant proportion of the research community who work on minimalist helical mimics base their designs on ideal secondary structures without stating a target PPI; this strategy affords generally interesting data because they mimic *ideal* secondary structures representative of the most common states found in proteins. For the reasons stated above, we decided ideal secondary structures should be the focus of our analysis here. However, the end of this paper relates the findings to some helical mimics that have been shown to perturb specific PPIs.

Amino acid Cα and Cβ coordinates are the best simple method for defining side-chain orientations. This is because setting a Cα–Cβ vector excludes many orientations of the "downstream" side-chain bonds; it would be *inappropriate* to use other side-chain vectors because Cβ–Cγ linkages and beyond are much less constrained. Overlaying Cα and Cβ side-chain coordinates may be used to access goodness of fit of a conformational state on a secondary structure in terms of RMSDs. This procedure has been used when applying Bartlett's CAVEAT algorithm,[35,36] Hamilton used it on his mimics of secondary structures,[6,27] and we have used it extensively too.[20,32,34]

Method for comparisons of scaffold conformations with ideal secondary structures

Preferred conformations of scaffolds that express only Cα and Cβ atoms, *i.e.* methyl substituted ones, show how the molecular core is biased to project amino acid side-chains. Any conformational state of all-methyl-substituted compounds may be approximated to three Cα–Cβ vectors or six (3 × Cα–Cβ) coordinates to represent how that state projects side-chains. Thus each conformation can be described in terms of irregular prismatic shapes formed by joining these coordinates (Fig. 2). Similarly, any set of three side-chains in an ideal secondary structure may be described in the same way.

Conformational populations are determined by a combination of kinetic and thermodynamic issues. It is only necessary to consider kinetic effects for semi-rigid small molecules if they have restricted rotation at ambient temperature that

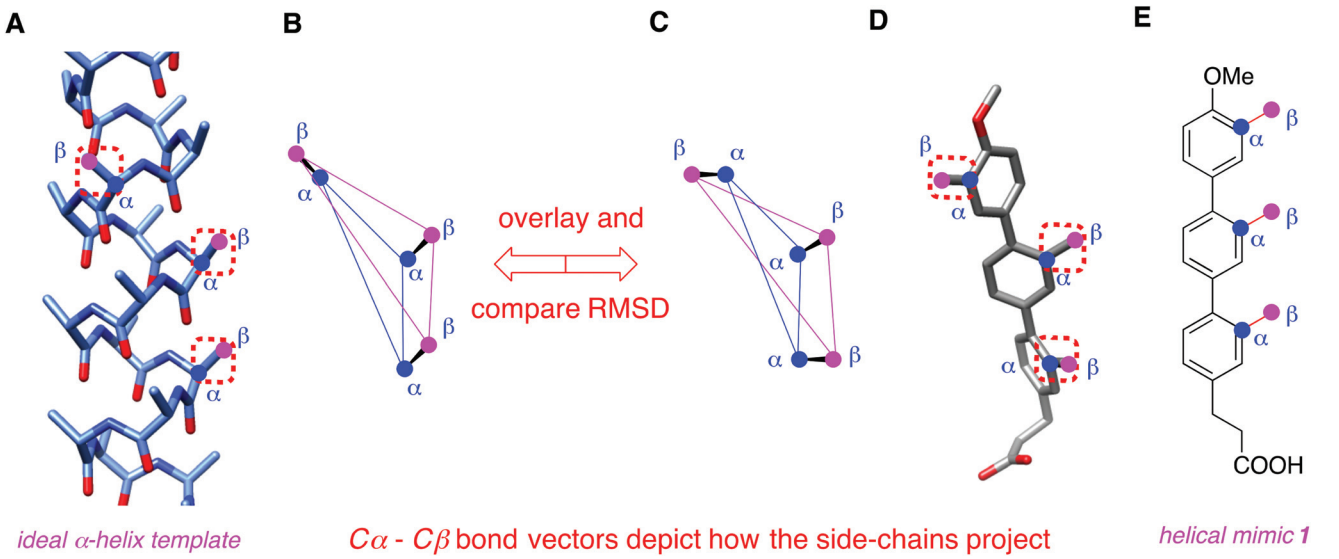

Fig. 2 Side-chain matching on secondary structures based on 3 × (Cα–Cβ) coordinates.

prevents equilibration between conformers; this is not the case for scaffolds **1–8**. To evaluate the thermodynamically favorable conformational states, we used Pettitt's QMD procedure.[37,38] Specifically, the scaffolds were minimized (molecular mechanics) then subjected to a molecular dynamics run at high temperature (1000 K) for 600 ps; 600 conformational states were thereby recorded during this run (*i.e.* one every 1 ps). These conformers were then minimized *via* molecular mechanics, but they were not clustered into families so that all the simulated conformers within 3 kcal mol^{-1} of the most stable identified were considered. Table 1 shows that in this strategy the number of accessible conformers generated for each mimic was 282 or more, implying that motions about each significant degree of freedom were explored in small increments by this conformer set. Thus all the accessible conformers generated in this way for each scaffold were systematically overlaid on every combination of side-chains in idealized secondary structures using procedures also used for the Exploring Key Orientations (EKO) approach as described.[32]

The prime objective of this work was to ascertain the bias of semi-rigid scaffolds **1–10** on secondary structures. Consequently, the medium used for the simulations was a constant (featureless) one of dielectric 80, corresponding to an aqueous environment. Explicit water molecules were not used because they would be displaced as the small molecule begins to interact with the protein-binding partner. Similarly, interactions between specific extended side-chains (*e.g.* Glu–Lys salt bridges) also tend to be nullified if these are interface side-chains that dock with a protein-binding partner. Assessing all the various side-chain to side-chain interactions that could occur therefore is unimportant for this method, besides being impractical. What is important is the conformations of semi-rigid scaffolds **1–10** with methyl side-chains, *i.e.* ones that reveal the intrinsic biases of the scaffolds.

Mimics **2**, **6** and **7** have *four*, not three, side-chains on the scaffold. For **2** the three side-chains highlighted in red (Fig. 1) were considered because these have different orientations to those in the terphenyl **1**. In **6** and **7** the side-chains chosen were two terminals and one internal because we estimated that combinations of this kind are most likely to resemble those on one face of a helix. Selection of those side-chains for **7** corresponds to the ones Arora originally used to generate overlays.

Six common ideal secondary structures were chosen for the overlay process (3_{10}-, α-, and π-helices; β-strands; parallel- and antiparallel β-sheets). Templates for ideal structures were obtained from Discovery Studio 2.5 (3_{10}-, α- and π-helices, and β-strands) and modified β-sheet builder (http://www-lbit.iro.umontreal.ca/bBuilder/index.html; parallel- and antiparallel-β-sheet and sheet/turn/sheets). Strand-turn-strand structures were also included, even though these are closely related to antiparallel β-sheets, because mimics **1–10** have extended structures that can simultaneously overlap with both the β-turn and β-sheet regions. Fig. 3 illustrates this, and is also intended to show that mimics can achieve optimal goodness-of-fit by overlaying on one strand or by "lying across" two or more regions in a sheet.

Table 1 Number of conformers below 3.0 kcal mol^{-1} for each mimic from QMD

Mimic	1	2	3	4	5	6	7	8	9	10
Number of conformers	600	599	567	469	282	507	299	421	600	490

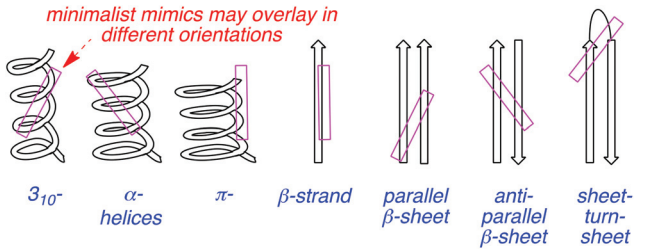

Fig. 3 Overlays considered in this paper place mimics on secondary structures in any orientation.

Comparisons of scaffold conformations with ideal secondary structures

Table 2 summarizes the lowest RMSDs obtained for fitting all the selected conformers for each mimic on ideal secondary structures. These data are colour coded to enable rapid evaluation of trends, but no absolute significance to the colour distinctions is implied. The one case that corresponded to an excellent fit is shaded in red, very good ones are shown in yellow, good ones are shown in green, and any "best-fit" with an RMSD of more than 0.70 Å is not shaded. To the best of our knowledge, there are no prior literature reports of minimalist mimics overlaid on α-helical motifs with RMSDs less than 0.70 Å, so these arbitrary delineations of "excellent", "very good", and "good" fits are relatively stringent.

Data in Table 2 are remarkable in several ways. As a whole they indicate some putative α-helical mimics actually have conformers that resemble β-strands, parallel and antiparallel β-sheets, and/or sheet-turn-sheets. Mimic **8** had no conformers that match any of the three helical types at RMSD 0.70 Å or less, but did have ones that fitted well on extended, sheet-related, conformations. Similarly, mimic **7** was shown to be a significantly better strand-turn-strand analog than it was for any of the helices, and the only helical structure that matched well was the rarer π-form. Hamilton's terphenyl mimic **1** gives better matches on 3_{10}- and π-helices than on the α-form, and overlaid unexpectedly well on a sheet-turn-sheet. In fact, the only very good α-helical mimic in the series was oligobenzamide **3**. Based on this analysis, scaffolds **3** and **4** appear to have the most potential as "universal mimics"[20] since they gave conformers that fit all six secondary structures well. However, this comparison is not even because it treats scaffolds **3**, **6**, and **8** in a *different* way to the others, for the reasons described below.

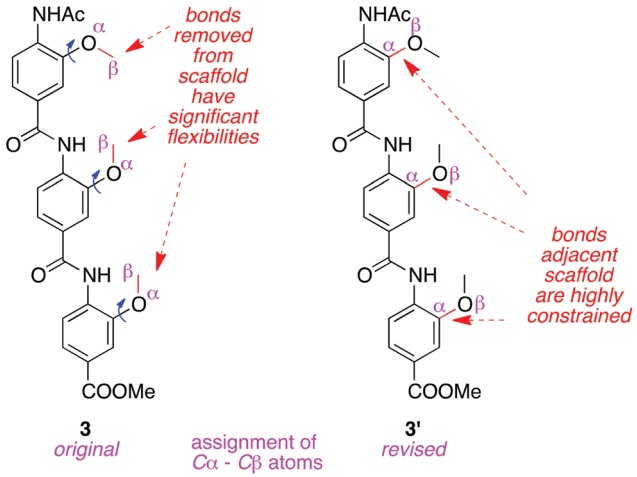

Fig. 4 Original and revised Cα and Cβ assignments illustrated for mimic **3**.

The bonds highlighted in red (Fig. 1) are the ones that the original researchers used to overlay with Cα–Cβ vectors. However, the highlighted bonds for mimics **1**, **2**, **4**, **5**, **7**, **9** and **10** are *directly* attached to the scaffold, but those for templates **3**, **6**, and **8** are *not*; at least one vector in the latter group of structures is one bond removed from the core. Thus the highlighted bonds in **3**, **6**, and **8** are closer to Cβ and Cγ atoms in a side-chain than to Cα and Cβσ hence they are less constrained than those in the other mimics (illustrated for the oligobenzamide scaffold in Fig. 4). A consequence of assigning Cα and Cβ bonds in the original way for **3**, **6**, and **8** is that this covers more conformational space than, for instance, structure **3′** that focuses on bonds *adjacent* the scaffold. This issue is accentuated for **3** and **6** because all three side-chains are of this type, whereas only one side-chain is impacted for **8** (*i.e.* the one involving the exocyclic amine).

As a result of the considerations above, conformational and matching analyses were repeated using structures **3′**, **6′**, and **8′** with Cα and Cβ assignments revised so that they correspond to

Table 2 Matching preferred conformations of scaffolds on ideal secondary structures[a]

	3_{10}-Helix	α-Helix	π-Helix	β-Strand	β-Sheet (parallel)	β-Sheet (anti-parallel)	Sheet-turn-sheet
1	0.65	0.71	0.59	—	—	—	0.58
2	0.39	0.59	0.78	—	0.89	0.81	0.84
3	0.30	0.31	0.47	0.70	0.58	0.43	0.43
4	0.36	0.51	0.55	0.57	0.60	0.59	0.59
5	0.60	0.51	0.55	—	—	—	0.54
6	0.60	0.61	0.57	0.96	0.93	0.90	0.51
7	0.81	0.72	0.51	1.05	0.89	0.95	0.36
8	0.74	0.80	0.85	—	0.61	—	0.61
9	0.82	0.79	0.91	0.65	0.41	0.69	0.44
10	0.58	0.78	0.63	0.73	0.42	0.55	0.46

[a] RMSD ≤ 0.30 Å, red background; 0.31–0.50 Å, yellow; 0.51–0.70 Å, green. RMSDs of over 1.1 Å are not shown.

Table 3 Matching preferred scaffold conformations using revised Cα and Cβ assignments[a]

	3_{10}-Helix	α-Helix	π-Helix	β-Strand	β-Sheet (parallel)	β-Sheet (anti-parallel)	Sheet-turn-sheet
3′	0.33	0.25	0.36	0.66	0.41	0.39	0.40
6′	0.59	0.66	0.70	—	—	—	0.53
8′	0.99	0.79	0.71	0.88	0.40	0.95	0.40

[a] RMSD ≤ 0.30 Å, red background; 0.31–0.50 Å, yellow; 0.51–0.70 Å, green.

vectors attached to the scaffold (Table 3). Under these conditions, all the mimics fit somewhat less well on most secondary structures, but conformers of the oligobenzamide system 3′ gave an excellent fit on the ideal α-helix. In fact, that was the best fit identified in this work for any mimic on any secondary structure.

Fig. 5a–d compares overlay data for the ten mimics for each of the three helical secondary structures, with an arbitrary

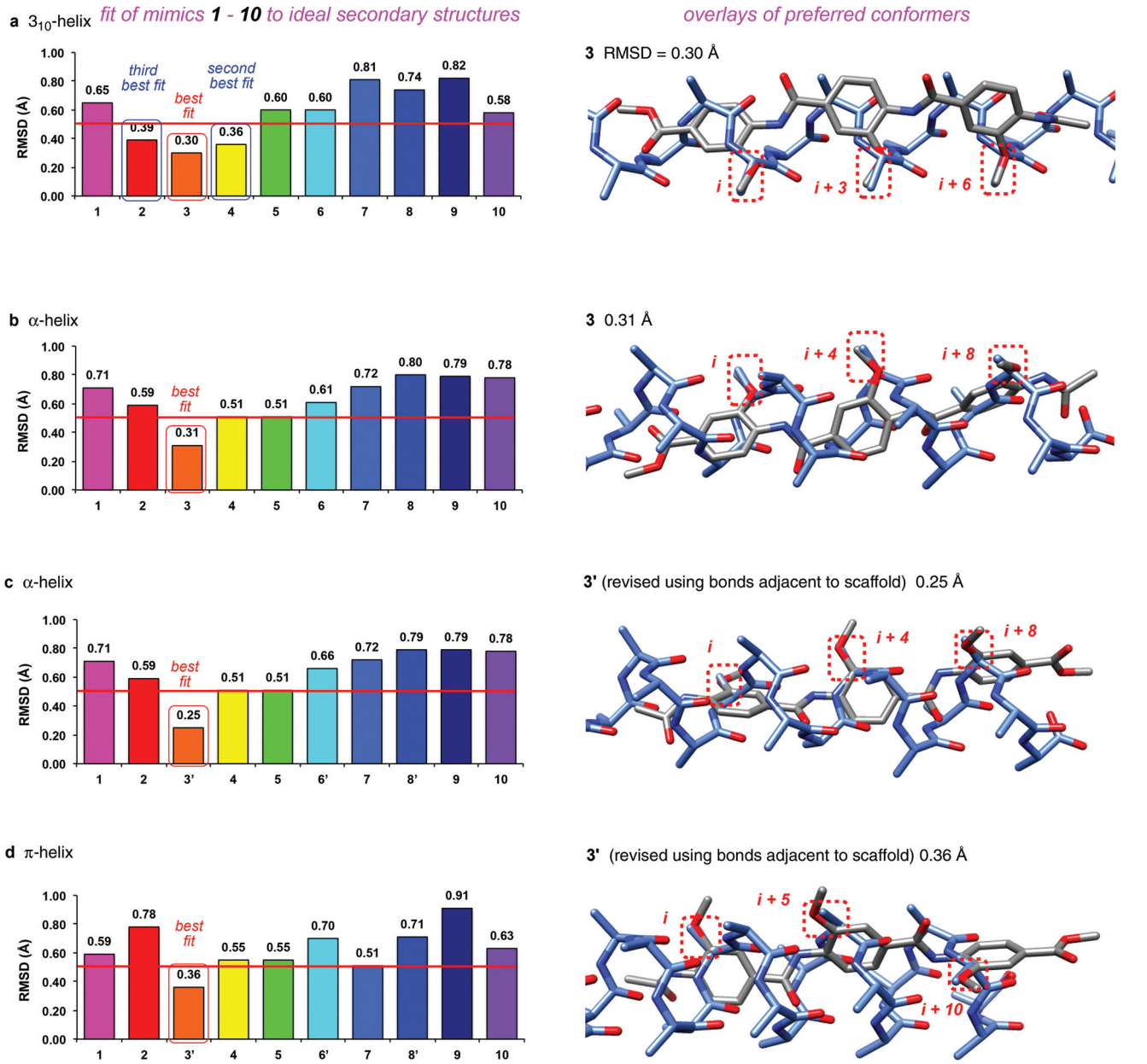

Fig. 5 Overlays of mimics **1–10** on ideal helical structures; the best match for each helical structure is shown on the right.

0.5 Å RMSD cutoff shown by a red line. Thus, for instance, Fig. 5a shows conformers of **3**, **4**, and **2** overlaid well on an ideal 3_{10}-helix relative to the other mimics; scaffold **3** gave the best overlay and this is shown on the right. Only the oligobenzamide system **3** overlaid with an RMSD of <0.5 Å on the ideal α-helix (5b), and the matching was improved when bonds adjacent the scaffold were considered (**3′**, 5c). Similarly, mimic **3′** (and **3**, overlay not shown but data in Table 2) gave the best overlays for the π-helix.

Fig. 6 shows overlay data for the mimics on extended, sheet-like structures. There were no good (<0.5 Å RMSD) correspondences for the ideal β-strand (6a). As expected, Smith's sheet mimic **9** and the pyrrolinones–pyrrolidine oligomer **10** both gave preferred conformers that matched parallel β-sheets almost equally well (6b). However, contrary to expectations: (i) the putative helical mimics **3′** and **8′** also match parallel β-sheets; (ii) scaffolds **9** and **10** do *not* overlay exceptionally well on anti-parallel β-sheets; and, (iii) the oligobenzamide mimic (analyzed using the **3′** or the **3** designation) populates conformers that *do* correspond to anti-parallel β-sheets.

Finally, mimic **7** was shown to have preferred conformers that overlay better on the sheet-turn-sheet than any other mimic; to do this it spans the two sheets and part of the turn region (6d). Scaffolds **3**, **3′**, **8′**, **9**, and **10** also had conformers that overlaid well on the sheet-turn-sheet motif.

The strategy used for comparing preferred conformations of the mimics with secondary structures described above does *not* consider the number of conformers that matched well

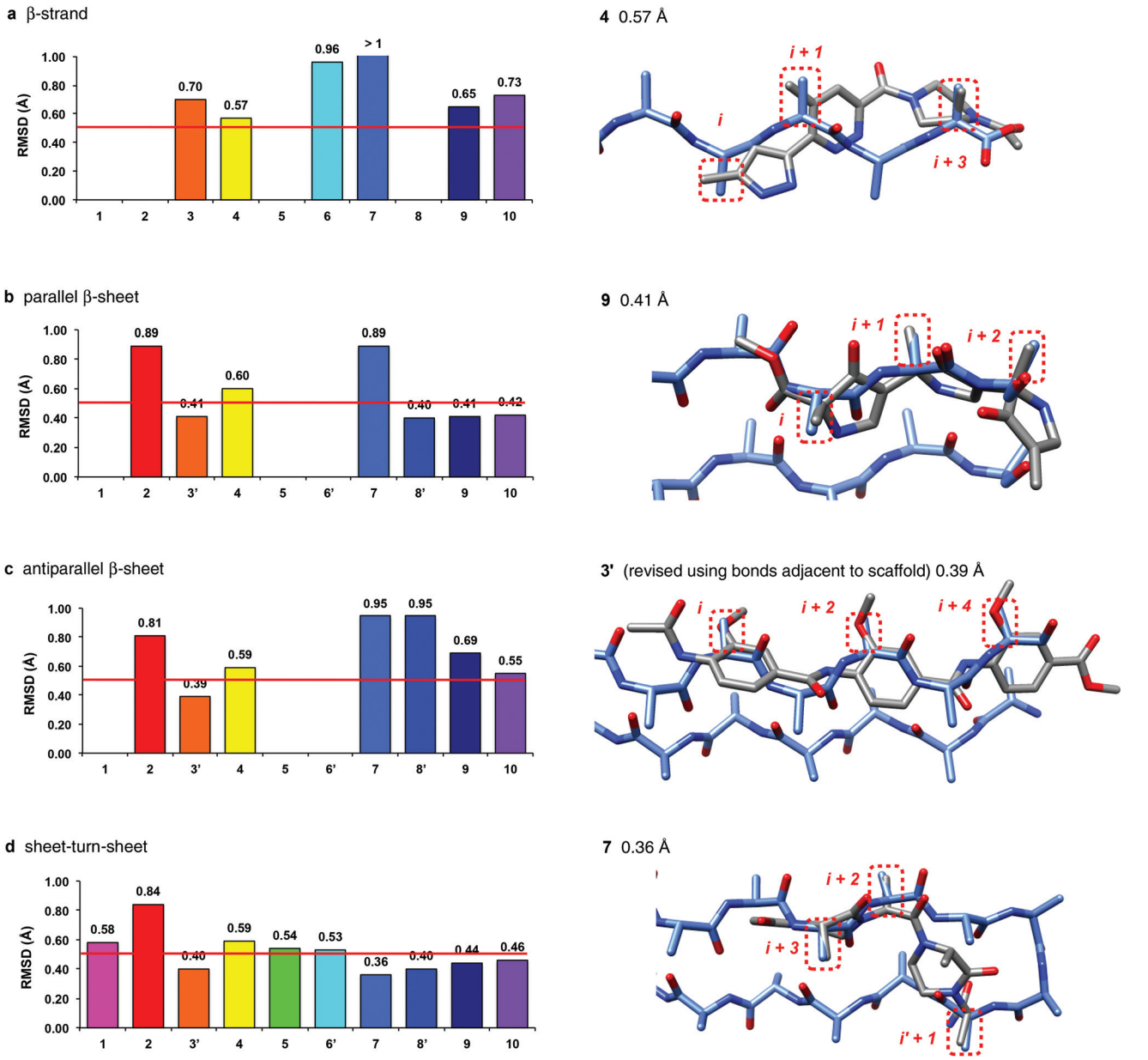

Fig. 6 Overlays of mimics **1–10** on ideal extended sheet-like structures; the best match for each motif is shown on the right.

(below RMSD 0.5 Å), or how much more energetic these matching conformers are relative to the lowest energy conformer detected (ΔE). To delve into these issues it is necessary to plot RMSDs *vs.* ΔEs for each conformer. This is done comprehensively in the ESI,† and Fig. 7 shows illustrative data.

Fig. 7 shows the distribution of conformers of the **3′** oligobenzamide description that overlay with 3_{10}-, α-, and π-helices at less than 1.0 Å RMSD and within 3 kcal mol^{-1} of the lowest energy form observed. All of the 3_{10}-helical conformers that did so with an RMSD of <0.5 Å had an *i*, *i* + 3, *i* + 6 side-chain correspondence (red dots boxed in red). Smith's analog **9** overlaid on a parallel β-sheet is shown for comparison. This scaffold is the most rigid in the series **1–10**, hence it is unsurprising that its conformers cluster tightly; in fact, they aggregate in approximately two groups, each with similar RMSDs. One of these conformational groups overlays parallel β-sheets well with a high population of low energy conformers.

Plots similar to those shown in Fig. 7, but for all the mimics, are shown in the ESI.† For brevity, this data is summarized in Table 4, which gives a semi-quantitative summary of all the dot-plot data for each scaffold type. For instance, no conformers were found for mimic **1** that were below 0.5 Å for overlay on any secondary structure (open circles for whole row), while mimic **10** had some conformers between 1.0 and 3.0 kcal mol^{-1} that overlaid with β-sheets or strand-turn-strand motifs (purple ticks). Conformers less than 1 kcal mol^{-1} above the minimum energy one that also matched ideal secondary structures with RMSDs of <0.5 Å were found for mimics **2**, **3** (and **3′**), **4**, **8**, and **9**.

Combinations of side-chains that best fit α-helical structures

Scaffolds **1–8** were originally designed to resemble α-helices. Overlays of each were shown by their discoverers to illustrate combinations of amino acid side-chains in the secondary structures that were presumed to match with preferred conformations of the mimics. These original assignments of side-chain combinations are shown in blue below each structure in Fig. 1. Shown in red are the side-chain combinations that correspond to the best overlay on an ideal α-helix as determined using our analysis. *Those assignments of side-chain combinations are different to the ones originally made for all the scaffolds shown*, except for Smith's β-sheet mimic. For our mimic **10** the procedure reported (by us) was the same as that used here,[34] so there is no difference.

Higher energy conformers were probed to determine if the side-chain combinations originally proposed for α-helix mimicry were present in our analyses at higher energies than the one with lowest RMSD. Data for this analysis are shown in Table 5.

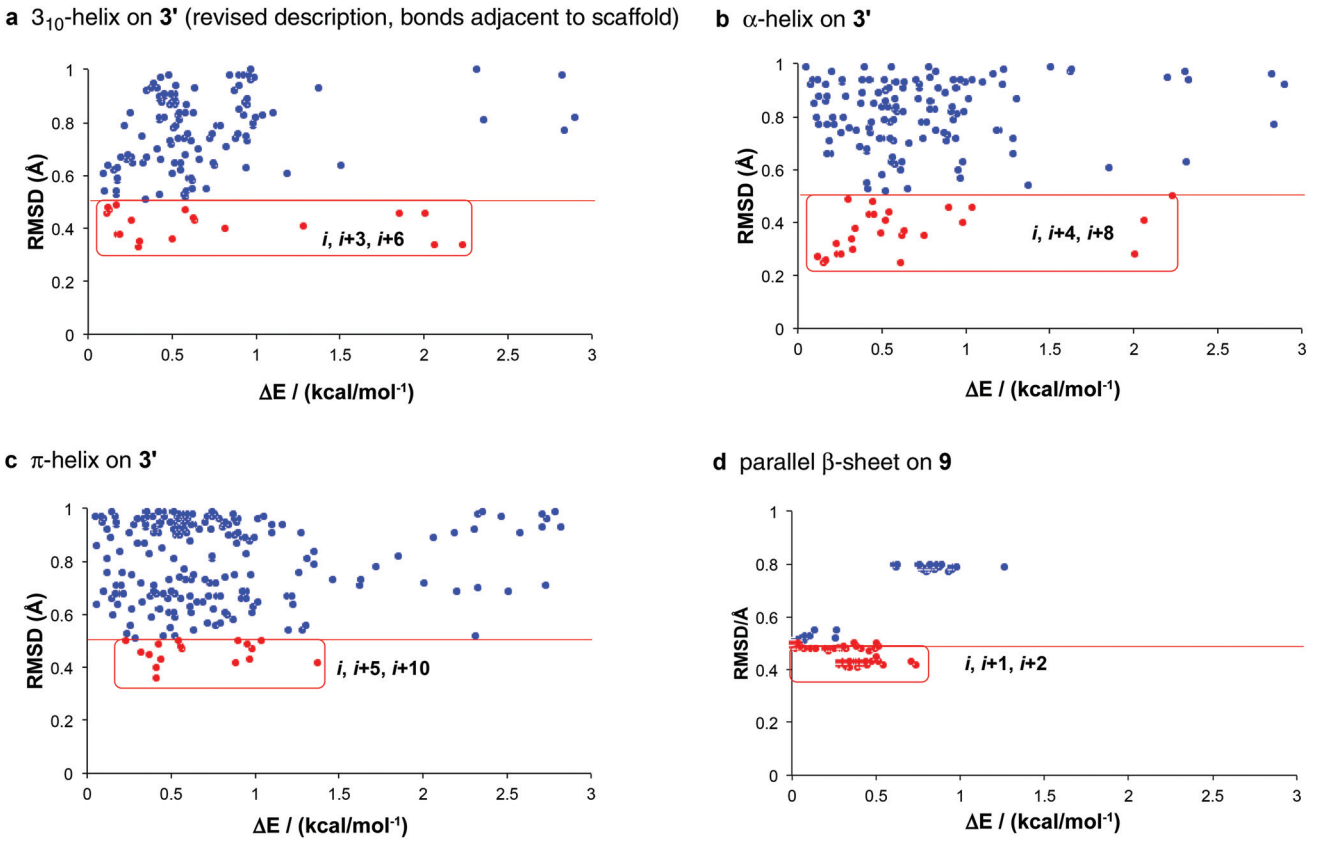

Fig. 7 Scatter plots of RMSD values of conformers *vs.* energies relative to the lowest energy conformer detected (ΔE) indicate how well each mimic populates the featured overlay states. The following numbers of conformers match the indicated secondary structures: (a) compound **3′** on 3_{10}-helix, 19 of 567 conformers, 3.4%; (b) compound **3′** on α-helix, 26/567, 4.6%; (c) compound **3′** on π-helix, 17/567, 3%; (d) compound **9** on β-sheet, 386/600, 64.3%.

Table 4 Summary of data from RMSD/ΔE scatter plots

	3_{10}-Helix	α-Helix	π-Helix	β-Strand	β-Sheet (parallel)	β-Sheet (anti-parallel)	Strand-turn-strand
1	O	O	O	O	O	O	O
2	✓✓	O	O	O	O	O	O
3	✓✓	✓✓	✓✓	O	O	✓✓	✓✓
3′	✓✓	✓✓	✓✓	O	✓✓	✓✓	✓✓
4	✓✓	O	O	O	O	O	O
5	O	O	O	O	O	O	O
6	O	O	O	O	O	O	O
6′	O	O	O	O	O	O	O
7	O	O	O	O	O	O	✓
8	O	O	O	O	O	O	O
8′	O	O	O	O	✓✓	O	✓✓
9	O	O	O	O	✓✓	O	✓✓
10	O	O	O	O	✓	O	✓

✓✓, RMSD < 0.50 Å and ΔE < 1.0 kcal mol^{-1}; ✓, RMSD < 0.50 Å and 1.0 kcal mol^{-1} < ΔE < 3.0 kcal mol^{-1}; O, RMSD > 0.50 Å.

Red combinations in Table 5 are those for the conformer with lowest RMSD overlay on an α-helix. Those shown in purple indicate favored conformations from our analyses that corresponded to side-chain combinations that are *different* to the most favorable conformation and necessarily have higher RMSDs. For instance, our analysis of mimic **1** found the overlay with the lowest RMSD corresponded to matching the *i*, *i* + 2, *i* + 5 α-helix side-chains. However, some other conformations of **1** matched three other side-chain sets with higher RMSD (*i*, *i* + 3, *i* + 5; *i*, *i* + 4, *i* + 5; *i*, *i* − 3, *i* − 5, the latter being an anti-parallel overlay on the secondary structure, *i.e.* one that opposes the *N*-to-*C* polarity). Absence of any side-chain combinations shown in blue for **1** indicates that *none* of the preferred conformers in our analysis corresponded to the amino acid side-chain combinations originally proposed (in this particular case that was *i*, *i* + 4, *i* + 7).

Overview of Table 5 shows *only one case* where a conformer was found that corresponded to the original assignment; specifically, one with an RMSD of 0.91 Å corresponding to the *i*, *i* + 3, *i* + 7 set originally proposed for mimic **4**. For comparison, Smith's sheet scaffold **9** was included and compared with a parallel β-sheet; the proposed side-chain combinations were identical to the exclusive one found *via* our analysis (thus could be shown in red or blue and were arbitrarily shown in blue).

Table 5 Side-chain combinations for preferred conformer with lowest RMSD relative to the α-helix (red), for other preferred conformations (purple; higher RMSD), and the side-chain combinations originally proposed for overlay (blue)

	Sequence correspondence for α-helices[a]
1	*i*, *i* + 2, *i* + 5; *i*, *i* + 3, *i* + 5; *i*, *i* + 4, *i* + 5; *i*, *i* − 3, *i* − 5
2	*i*, *i* + 2, *i* + 3
3	*i*, *i* + 4, *i* + 8; *i*, *i* + 4, *i* + 9; *i*, *i* + 5, *i* + 8; *i*, *i* − 4, *i* − 8
3′	*i*, *i* + 4, *i* + 8
4	*i*, *i* + 3, *i* + 5; *i*, *i* + 2, *i* + 5; *i*, *i* + 4, *i* + 6; *i*, *i* + 2, *i* + 6; *i*, *i* − 1, *i* − 5; *i*, *i* + 3, *i* + 6; ***i***, ***i*** + 3, ***i*** + 7 (0.91)
5	*i*, *i* + 2, *i* + 5; *i*, *i* + 1, *i* + 5; *i*, *i* − 4, *i* − 5; *i*, *i* + 3, *i* + 5; *i*, *i* + 4, *i* + 5; *i*, *i* − 3, *i* − 5
6	*i*, *i* + 2, *i* + 6; *i*, *i* − 2, *i* − 6
6′	*i*, *i* − 1, *i* − 5; *i*, *i* + 1, *i* + 5
7	*i*, *i* + 1, *i* + 3; *i*, *i* + 1, *i* + 5; *i*, *i* − 1, *i* − 3; *i*, *i* − 1, *i* + 3; *i*, *i* + 3, *i* + 5; *i*, *i* − 3, *i* − 6; *i*, *i* + 1, *i* − 3; *i*, *i* − 1, *i* + 2; *i*, *i* − 1, *i* − 5; *i*, *i* + 2, *i* + 4; *i*, *i* + 1, *i* + 4
8	*i*, *i* + 4, *i* + 5; *i*, *i* − 4, *i* − 5; *i*, *i* + 2, *i* + 5; *i*, *i* − 3, *i* − 5; *i*, *i* + 3, *i* + 5
8′	*i*, *i* + 1, *i* + 2; *i*, *i* − 1, *i* − 2
9	*i*, *i* + 1, *i* + 2 for parallel β-sheet
10	*i*, *i* + 4, *i* + 8; *i*, *i* + 1, *i* + 5; *i*, *i* + 2, *i* + 6; *i*, *i* + 3, *i* + 7; *i*, *i* + 4, *i* + 7

[a] Red indicates amino acid side-chain combinations for the best matching conformer found in this work; purple indicates other conformers found in this work; blue indicates amino acid side-chain combinations indicated for the original publications. Designations with negatives, *e.g.* *i*, *i* − 3, *i* − 5, indicate conformations that overlay antiparallel to the *N*-to-*C* orientation in the secondary structure.

Helical mimics do not need to be ideal to perturb protein–protein interactions

In several cases, helical mimics featured in this paper have been made and tested for their ability to perturb PPIs that involve a helix at an interface. Specifically, the PPIs shown in Table 6 have been assayed using mimics **1**,[39] **3**,[29,40] and **8** (p53/MDM2),[16] **1** (smMLCK/calmodulin),[4] **1**[5,6] and **3**[29] (BakBH3/Bcl-x_L), and **1**[41] (gp41, *C*-/*N*-helical region).[42] Red-shaded regions in Table 6 indicate overlays with low RMSD values while yellow- and green-colored ones, respectively, fitted less well.

Table 6 also indicates side-chain correspondences colored to show how they correspond to those predicted here for *ideal* secondary structures, and with the predictions in the original papers. Thus in several cases the side-chain correspondences observed when all conformers of the mimics were overlaid on the PPI helical motifs did *not* match either the predictions based on ideal secondary structures (Table 2) or the ones made in the original work; these are shown in black in Table 6. However, in the majority of cases (shown in red) the side-chain correlations did match those predicted here for ideal secondary structures. In one case, shown in blue for mimic **3** overlaid on p53/MDM2, only the original prediction coincided with the side-chain correlations found by our overlay procedure applied to the interface helical motifs.

Table 6 RMSD values for preferred mimic conformations overlaid on PPI components[a]

PPI	1	2	3	3′	4	5	6	6′	7	8	8′	9	10
p53/MDM2[b]	0.57 *i*, *i* + 2, *i* + 3	0.66 *i*, *i* + 2, *i* + 3	0.46 *i*, *i* + 4, *i* + 7	0.55 *i*, *i* + 4, *i* + 7	0.51 *i*, *i* + 3, *i* + 6	0.54 *i*, *i* + 1, *i* + 3	0.50 *i*, *i* + 2, *i* + 4	0.59 *i*, *i* + 4, *i* + 5	0.34 *i*, *i* + 1, *i* + 3	0.43 *i*, *i* + 2, *i* + 3	0.33 *i*, *i* + 1, *i* + 2	0.34 *i*, *i* + 1, *i* + 2	0.47 *i*, *i* + 4, *i* + 8
smMLCK/calmodulin[c]	0.68 *i*, *i* + 2, *i* + 5	0.60 *i*, *i* + 2, *i* + 3	0.25 *i*, *i* + 4, *i* + 8	0.21 *i*, *i* + 4, *i* + 8	0.35 *i*, *i* + 3, *i* + 5	0.52 *i*, *i* + 2, *i* + 5	0.52 *i*, *i* + 2, *i* + 6	0.57 *i*, *i* + 4, *i* + 5	0.57 *i*, *i* + 6, *i* + 5	0.65 *i*, *i* + 4, *i* + 5	0.77 *i*, *i* + 1, *i* + 2	0.68 *i*, *i* + 1, *i* + 3	0.68 *i*, *i* + 4, *i* + 8
BakBH3/Bcl-x_L[d]	0.61 *i*, *i* + 3, *i* + 5	0.67 *i*, *i* + 2, *i* + 3	0.28 *i*, *i* + 3, *i* + 7	0.42 *i*, *i* + 4, *i* + 8	0.45 *i*, *i* + 3, *i* + 6	0.61 *i*, *i* + 1, *i* + 4	0.47 *i*, *i* + 2, *i* + 5	0.59 *i*, *i* + 4, *i* + 5	0.43 *i*, *i* + 1, *i* + 3	0.90 *i*, *i* + 4, *i* + 5	0.59 *i*, *i* + 1, *i* + 2	0.23 *i*, *i* + 1, *i* + 2	0.49 *i*, *i* + 4, *i* + 8
gp41*C*-/*N*-helical region[e]	0.73 *i*, *i* + 3, *i* + 5	0.55 *i*, *i* + 2, *i* + 3	0.28 *i*, *i* + 4, *i* + 8	0.26 *i*, *i* + 4, *i* + 8	0.40 *i*, *i* + 3, *i* + 5	0.46 *i*, *i* + 2, *i* + 5	0.54 *i*, *i* + 2, *i* + 6	0.62 *i*, *i* + 4, *i* + 5	0.58 *i*, *i* + 1, *i* + 3	0.71 *i*, *i* + 4, *i* + 5	0.73 *i*, *i* + 1, *i* + 2	0.60 *i*, *i* + 1, *i* + 2	0.72 *i*, *i* + 4, *i* + 8
Predicted from ideal secondary structures	*i*, *i* + 2, *i* + 5	*i*, *i* + 2, *i* + 3	*i*, *i* + 4, *i* + 8	*i*, *i* + 4, *i* + 8	*i*, *i* + 3, *i* + 5	*i*, *i* + 2, *i* + 5	*i*, *i* + 2, *i* + 6	*i*, *i* + 4, *i* + 5	*i*, *i* + 1, *i* + 3	*i*, *i* + 4, *i* + 5	*i*, *i* + 1, *i* + 2	*i*, *i* + 1, *i* + 2	*i*, *i* + 4, *i* + 8
Predicted originally	*i*, *i* + 4, *i* + 7	*i*, *i* + 3, *i* + 4	*i*, *i* + 4, *i* + 7	—	*i*, *i* + 3, *i* + 7	*i*, *i* + 3, *i* + 7	*i*, *i* + 2, *i* + 7	—	*i*, *i* + 4, *i* + 7	*i*, *i* + 3, *i* + 7	—	*i*, *i* + 1, *i* + 2	*i*, *i* + 4, *i* + 8

[a] Red background RMSD ≤ 0.30 Å; 0.30 Å < RMSD ≤ 0.50 Å, yellow; 0.50 Å < RMSD ≤ 0.70 Å, green. Side-chain correspondences shown in black did not correspond to the original predictions or those from matching ideal secondary structures as described here, blue denotes correspondence to the original prediction, and red indicates correspondence to the matches deduced here. [b] Helical component shown first throughout; PDB identifier, 1YCR. [c] 1CDL. [d] 1BXL. [e] 1AIK.

Most of the data shown in Table 6 corresponds to mimic/PPI combinations that have *not* been assayed so far. In two cases a mimic/PPI interface combination seems mutually well suited. In the first, mimic **3** is matched well with BakBH3/Bcl-x_L,[43] gp41, and smMLCK/calmodulin, but tests have only been reported for the first. Second, and surprisingly, Smith's system **9** shows an excellent match for the BakBH3/Bcl-x_L; no assays have been reported for this since it has, until now, been regarded as exclusively a β-sheet mimic. Closer examination reveals this overlay is on a helical-terminus where the conformation begins to unwind (see ESI†).

Data in Table 6 do *not* mean that the authors of the original papers should have chosen different side-chain correspondences, for various reasons. For instance, some of the side-chains that overlay well when our conformational search routine is used point away from the interface. Thus Table 6 should only be used to select mimics to disrupt those PPIs after the orientation of the mimic side-chains have been checked to see if they are appropriate to interact with the protein-binding partner.

Differences between the data in Table 2 (RMSDs for overlays on *ideal* secondary structures) and **6** (on *actual* PPI interfaces) reflect the fact that secondary structures in proteins are not ideal. For instance, Table 2 indicates mimics **7**–**10** are relatively poor helical mimics, but they overlay on the p53/MDM2 interface with RMSDs that are superior to nearly every entry in Table 2 for matching all the mimics on any ideal secondary structure.

Finally, even if a mimic displaces a helical protein fragment at a PPI this does *not* prove that the small molecule binds in a helical conformation, and it is hard to confirm that it does by most methods. Binding of a helical mimic to a receptor pocket for a protein helix gives only circumstantial evidence. Hamilton *et al.* proved various terphenyls **1** could influence the interaction of calmodulin with the α-helical domain of smooth muscle myosin light-chain kinase,[4] and used the same scaffold to perturb the α-helical binding domain of Bak BH3 interacting with Bcl-x_L (selectively over p53/HDM2).[6] In the former case the compound was used as a *i*, *i* + 3 and *i* + 7 mimic, but as a *i*, *i* + 4 and *i* + 7 mimic in the latter case. HSQC experiments with ^{15}N-labeled Bcl-x_L proved the mimic bound in that binding cleft.[6] Such HSQC experiments are a gold standard in the field; they confirm a mimic binds in the targeted region, and that is still rare in the field of minimalist mimics of secondary structures.[44] In Hamilton's studies those experiments proved the terphenyl associates with the hydrophobic cavity where the helical BH3 peptide binds, but the perturbation of protein ^{15}N-chemical shifts on binding does not reveal the conformation of the bound mimic. Moreover, Hamilton's docking studies indicated the terphenyl mimic could occupy the same hydrophobic cleft as Bak in Bcl-x_L but in a slightly different orientation. In Hamilton's work it was not critical to elucidate the exact binding mode since they achieved their objective: to find a small molecule to perturb Bak/Bcl-x_L. However, for helical mimicry in general, the conformation of the small molecule bound to the protein is interesting. This would require crystallography of the complex, and no group has reported such X-ray data for any of the mimics **1**–**8**. That type of crystallographic data can be hard to obtain for

compounds that bind one protein component with low affinity, and for PPIs where the isolated proteins have different structures compared with the PPI complex.

Conclusions

Computational simulations of rapidly equilibrating conformational states of minimalist mimics in solution reveal information that cannot be obtained *via* direct spectroscopic measurements. Preferred simulated conformations of methyl-substituted scaffolds in a continuous dielectric of 80 represent the intrinsic bias of that scaffold with methyl groups in the absence of explicit water molecules. In other words, they represent how the scaffold-core is bias to project Cα–Cβ vectors as it surrenders water of solvation and begins to interact with a protein-binding partner.

Orientations of Cα and Cβ atoms in preferred conformations of minimalist mimics can be related to the same vectors in secondary structures by automated overlay routines. Computational methods like this can be repeated for hundreds of conformers, making it possible to evaluate a whole conformational ensemble in terms of quantitative RMSD outputs; this is faster and more reliable than could ever be achieved by matching two 3D molecules "by eye" based on a 2D representation on a screen, or by docking a few conformations from large ensembles *via* MD simulation routines. The key innovation in the research described here is to introduce this type of procedure as a means to evaluate the general applicability of the featured compound types in secondary structure and interface mimicry.

There have been so many papers on minimalist helical mimics that readers who do not follow the field might assume the major challenges must have been surmounted, but this study convinced us that the opposite is true. It is difficult to relate the mimics to their preferred side-chain correspondences, and there are many side-chain correspondences which, based on these simulations, cannot be matched by any of the mimics **1–10** with an RMSD of less than 0.5 Å. It would be optimal to have at least one minimalist mimic that can attain a good match (arbitrarily this might be 0.5 Å RMSD) for each side-chain correspondence in every secondary structure, but this has not been achieved. Within the constraints of the methods presented here (limitations of the force fields, assumptions regarding the media for simulations) our simulations indicate that the best mimic of an α-helix is **3**, and that happens to correspond to i, $i + 4$, $i + 8$ side-chain orientations (RMSD of 0.31). In fact, none of the other helical mimics cover other side-chain combinations with an RMSD of <0.50. Another challenge in the field of helical mimicry is to improve the suitability of helical mimics for applications as cell permeable chemical probes and pharmaceutical leads. Compounds containing scaffold **3**, for instance, are unlikely to be cell permeable due to the amide *H*-bond donors. There are ample opportunities for refined design of minimalist secondary structure mimics.

Simulated conformational equilibria of the featured scaffolds reveals that many err towards being universal mimics[20] (several secondary structures represented in one conformational ensemble). Thus, the compounds have the potential to be used as α-helical mimics and to resemble other secondary structures; the featured scaffolds might be used in ways that may not have been obvious before.

Some of the mimics **1–8** were probably conceived to match non-ideal helices at specific PPI interfaces. Simulations here indicate that many of the featured helical mimics cannot access conformations that overlay well (*e.g.* <0.5 Å RMSD) with *ideal* secondary structures, but *can* match distorted helices at particular PPI interfaces. In general, research focused on perturbing PPIs requires close consideration of side-chain orientations *at the particular targeted interface*. We feel that this is the direction the field is already moving in: design and synthesis of *interface mimics*, rather than secondary structure mimics. However, it does not matter if the target conformation is an ideal secondary structure or a completely "non-classical" observed at a PPI, simulations of the type outlined here will be valuable because evaluation of minimalist mimic conformations with PPI target conformations can reveal information that is not conveniently obtained *via* spectroscopy. This is, of course, especially true for predictive work to evaluate potential interface mimics before they have been prepared (*cf.* Table 6). Thus simulations such as these are a possible opening steps in a process that should be followed by checking for the absence of unfavorable backbone interactions of the scaffold with the protein receptor, syntheses, binding assays, and determination of the site of binding.

Acknowledgements

We thank The National Institutes of Health (GM087981) and The Robert A. Welch Foundation (A-1121) for financial support.

References

1 E. Ko, J. Liu and K. Burgess, *Chem. Soc. Rev.*, 2011, **40**, 4411–4421.
2 L. L. Conte, C. Chothia and J. Janin, *J. Mol. Biol.*, 1999, **285**, 2177–2198.
3 C. A. Lipinski, F. Lombardo, B. W. Dominy and P. J. Feeney, *Adv. Drug Delivery Rev.*, 1997, **23**, 3–25.
4 B. P. Orner, J. T. Ernst and A. D. Hamilton, *J. Am. Chem. Soc.*, 2001, **123**, 5382–5383.
5 O. Kutzki, H. S. Park, J. T. Ernst, B. P. Orner, H. Yin and A. D. Hamilton, *J. Am. Chem. Soc.*, 2002, **124**, 11838–11839.
6 H. Yin, G. Lee, K. A. Sedey, O. Kutzki, H. S. Park, B. P. Orner, J. T. Ernst, H.-G. Wang, S. M. Sebti and A. D. Hamilton, *J. Am. Chem. Soc.*, 2005, **127**, 10191–10196.
7 I. C. Kim and A. D. Hamilton, *Org. Lett.*, 2006, **8**, 1751–1754.

8 J.-M. Ahn and S.-Y. Han, *Tetrahedron Lett.*, 2007, **48**, 3543–3547.
9 A. Shaginian, L. R. Whitby, S. Hong, I. Hwang, B. Farooqi, M. Searcey, J. Chen, P. K. Vogt and D. L. Boger, *J. Am. Chem. Soc.*, 2009, **131**, 5564–5572.
10 J. Plante, F. Campbell, B. Malkova, C. Kilner, S. L. Warriner and A. J. Wilson, *Org. Biomol. Chem.*, 2008, **6**, 138–146.
11 A. Volonterio, L. Moisan and J. Rebek, Jr., *Org. Lett.*, 2007, **9**, 3733–3736.
12 L. Moisan, S. Odermatt, N. Gombosuren, A. Carella and J. Rebek, Jr., *Eur. J. Org. Chem.*, 2008, 1673–1676.
13 P. Maity and B. Koenig, *Org. Lett.*, 2008, **10**, 1473–1476.
14 S. Marimganti, M. N. Cheemala and J.-M. Ahn, *Org. Lett.*, 2009, **11**, 4418–4421.
15 P. Tosovska and P. S. Arora, *Org. Lett.*, 2010, **12**, 1588–1591.
16 H. Lee Ji, Q. Zhang, S. Jo, C. Chai Sergio, M. Oh, W. Im, H. Lu and H.-S. Lim, *J. Am. Chem. Soc.*, 2011, **133**, 676–679.
17 H. Yin, G.-I. Lee and A. D. Hamilton, *Drug Discovery Res.*, 2007, 281–299.
18 J. M. Davis, L. K. Tsou and A. D. Hamilton, *Chem. Soc. Rev.*, 2007, **36**, 326–334.
19 V. Azzarito, K. Long, N. S. Murphy and A. J. Wilson, *Nat. Chem.*, 2013, **5**, 161–173.
20 E. Ko, J. Liu, L. M. Perez, G. Lu, A. Schaefer and K. Burgess, *J. Am. Chem. Soc.*, 2011, **133**, 462–477.
21 A. Bax and D. G. Davis, *J. Magn. Reson.*, 1985, **63**, 207–213.
22 H. Kessler, C. Griesinger, R. Kerssebaum, K. Wagner and R. R. Ernst, *J. Am. Chem. Soc.*, 1987, **109**, 607–609.
23 P. Prabhakaran, V. Azzarito, T. Jacobs, M. J. Hardie, C. A. Kilner, T. A. Edwards, S. L. Warriner and A. J. Wilson, *Tetrahedron*, 2012, **68**, 4485–4491.
24 K.-Y. Jung, K. Vanommeslaeghe, E. Lanning Maryanna, L. Yap Jeremy, C. Gordon, T. Wilder Paul, D. Mackerell Alexander Jr. and S. Fletcher, *Org. Lett.*, 2013, **15**, 3234–3237.
25 S. Marimganti, M. N. Cheemala and J.-M. Ahn, *Org. Lett.*, 2009, **11**, 4418–4421.
26 O. V. Kulikov and A. D. Hamilton, *RSC Adv.*, 2012, **2**, 2454–2461.
27 C. L. Sutherell, S. Thompson, R. T. W. Scott and A. D. Hamilton, *Chem. Commun.*, 2012, **48**, 9834–9836.
28 F. Mohamadi, N. G. J. Richards, W. C. Guida, R. Liskamp, M. Lipton, C. Caufield, G. Chang, T. Hendrickson and W. C. Still, *J. Comput. Chem.*, 1990, **11**, 440–467.
29 V. Azzarito, P. Prabhakaran, A. I. Bartlett, N. S. Murphy, M. J. Hardie, C. A. Kilner, T. A. Edwards, S. L. Warrinera and A. J. Wilson, *Org. Biomol. Chem.*, 2012, **10**, 6469–6472.
30 J. C. Fuller, R. M. Jackson, T. A. Edwards, A. J. Wilson and M. R. Shirts, *PLoS One*, 2012, **7**, e43253.
31 J. L. Yap, X. Cao, K. Vanommeslaeghe, K.-Y. Jung, C. Peddaboina, P. T. Wilder, A. Nan, A. D. MacKerell, W. R. Smythe and S. Fletcher, *Org. Biomol. Chem.*, 2012, **10**, 2928–2933.
32 E. Ko, A. Raghuraman, L. M. Perez, T. R. Ioerger and K. Burgess, *J. Am. Chem. Soc.*, 2013, **135**, 167–173.
33 A. B. Smith, III, A. K. Charnley and R. Hirschmann, *Acc. Chem. Res.*, 2011, **44**, 180–193.
34 A. Raghuraman, E. Ko, L. M. Perez, T. R. Ioerger and K. Burgess, *J. Am. Chem. Soc.*, 2011, **133**, 12350–12353.
35 W. W. Smith and P. A. Bartlett, *J. Am. Chem. Soc.*, 1998, **120**, 4622–4628.
36 G. Lauri and P. A. Bartlett, *J. Comput.-Aided Mol. Des.*, 1994, **8**, 51–66.
37 B. M. Pettitt, T. Matsunaga, F. Al-Obeidi, C. Gehrig, V. J. Hruby and M. Karplus, *Biophys. J.*, 1991, **60**, 1540–1544.
38 S. D. O'Connor, P. E. Smith, F. Al-Obeidi and B. M. Pettitt, *J. Med. Chem.*, 1992, **35**, 2870–2881.
39 H. Yin, G.-i. Lee, H. S. Park, G. A. Payne, J. M. Rodriguez, S. M. Sebti and A. D. Hamilton, *Angew. Chem., Int. Ed.*, 2005, **44**, 2704–2707.
40 J. P. Plante, T. Burnley, B. Malkova, M. E. Webb, S. L. Warriner, T. A. Edwards and A. J. Wilson, *Chem. Commun.*, 2009, 5091–5093.
41 J. T. Ernst, O. Kutzki, A. K. Debnath, S. Jiang, H. Lu and A. D. Hamilton, *Angew. Chem., Int. Ed.*, 2002, **41**, 278–281.
42 P. Ravindranathan, T.-K. Lee, L. Yang, M. M. Centenera, L. Butler, W. D. Tilley, J.-T. Hsieh, J.-M. Ahn and G. V. Raj, *Nat. Commun.*, 2013, **4**, 1–11.
43 J.-M. Ahn, *US patent*, 20090113, 2010.
44 F. Campbell, J. P. Plante, T. A. Edwards, S. L. Warriner and A. J. Wilson, *Org. Biomol. Chem.*, 2010, **8**, 2344–2351.